IOP Publishing | Institute of Physics and Engineering in Medicine Physics in Medicine & Biology
Phys. Med. Biol. **00** (2014) 1–25 UNCORRECTED PROOF

A critical study of different Monte Carlo scoring methods of dose average linear-energy-transfer maps calculated in voxelized geometries irradiated with clinical proton beams

M A Cortés-Giraldo[1] and A Carabe[2]

[1] Department of Atomic, Molecular and Nuclear Physics, Universidad de Sevilla, Seville, Spain
[2] Department of Radiation Oncology, Hospital of The University of Pennsylvania, Philadelphia, PA, USA

E-mail: miancortes@us.es

Received 2 June 2014, revised 24 September 2014
Accepted for publication 21 October 2014
Published

Abstract

We compare unrestricted dose average linear energy transfer (LET) maps calculated in voxelized geometries irradiated with proton therapy beams with three different Monte Carlo scoring methods. Simulations were done with the Geant4 (Geometry ANd Tracking) toolkit. The first method corresponds to a step-by-step computation of LET which has been reported previously in the literature. We found that this scoring strategy is influenced by spurious high LET components, which significantly increases as the voxel size becomes smaller. Dose average LET values calculated for primary protons in water with voxel size of 0.2 mm were a factor ~1.8 higher than those obtained with a size of 2.0 mm at the plateau region for a 160 MeV beam. Such high LET components are a consequence of proton steps in which the condensed-history algorithm determines an energy transfer to an electron of the material close to the maximum value, while the step length remains limited due to voxel boundary crossing. Two alternative methods were derived to overcome this problem. The second scores LET along the entire path described by each proton within the voxel. The third followed the same approach of the first method, but the LET was evaluated at each step from stopping power tables according to the proton kinetic energy value. We carried out microdosimetry calculations with the aim of deriving reference dose average LET values from microdosimetric quantities. Significant differences between the methods were reported either with pristine or spread-out Bragg peaks (SOBPs). The first method reported

JNL:PMB PIPS: 504538 TYPE: PAP TS: NEWGEN DATE:12/11/14 EDITOR: AT SPELLING: UK

values systematically higher than the other two at depths proximal to SOBP by about 15% for a 5.9 cm wide SOBP and about 30% for a 11.0 cm one. At distal SOBP, the second method gave values about 15% lower than the others. Overall, we found that the third method gave the most consistent performance since it returned stable dose average LET values against simulation parameter changes and gave the best agreement with dose average LET estimations from microdosimetry calculations.

Keywords: proton therapy, LET, Monte Carlo simulation, Geant4

(Some figures may appear in colour only in the online journal)

AQ1

1. Introduction

Proton and carbon therapy have become more wide spread radiation therapy techniques in the recent years (Delaney and Kooy 2008, Schardt *et al* 2010). The potential advantages offered by light-ion beams regarding dose conformality over photon beams and recent technological advances have motivated the growth in the number of institutions offering such therapies, with others being currently in construction or planned (PTCOG). AQ2

Furthermore, protons and carbon ions offer a cell-killing effectiveness higher than photons for the same level of absorbed dose. This quality is often quantified in terms of a factor, relative biological effectiveness (RBE), which converts absorbed dose into biological dose (IAEA 2008). The RBE depends on physical properties, such as dose or radiation quality, and with biological aspects such as tissue type or endpoint considered (Belli *et al* 1998, Belli *et al* 2000, Furusawa *et al* 2000, Gerweck and Kozin 1999, Goodhead *et al* 1992, Paganetti *et al* 2002, AQ3 Wouters *et al* 1996).

Currently, the knowledge of biological parameters is limited. Thus, most RBE models use beam properties as input data and introduce phenomenological parameters to encompass the tissue response. Radiation quality has been characterized either from a microscopic approach, such as track-structure (Paganetti and Goitein 2001) and microdosimetry analysis (Hawkins 2003, Lindborg *et al* 2013, Burigo *et al* 2014), or with macroscopic models, usually in terms of linear energy transfer (LET) or dose average LET ($\overline{L}_{\mathrm{d}}$) (Wilkens and Oelfke 2004, Carabe *et al* 2013).

A constant RBE value of 1.1 is clinically recommended for protons, although it is well known that the RBE can be larger, especially at distal Bragg peak region (Matsuura *et al* 2010). Thus, recent works aim at using dose and $\overline{L}_{\mathrm{d}}$ objective functions to optimize proton plans in order to increase the biological effectiveness of proton treatments (Frese *et al* 2011, Giantsoudi *et al* 2013, Fager *et al* 2014). This approach has been called 'LET-painting' (Bassler *et al* 2010). These works take advantage of the monotonic dependence that RBE has in terms of LET for clinical proton beams. For heavier ions, the RBE decreases at high values of LET due to the overkill effect (Barendsen 1994); thus, the so-called LET-painting with carbon ions is not as straightforward as with protons.

The calculation of restricted and unrestricted $\overline{L}_{\mathrm{d}}$ distributions in clinical proton beams has been carried out either by means of analytical models (Wilkens and Oelfke 2003, Kempe *et al* 2007) and Monte Carlo simulations (Grassberger and Paganetti 2011, Kantemiris *et al* 2011, Romano *et al* 2014). In both approaches, $\overline{L}_{\mathrm{d}}$calculations have been done based on fluence evaluation of primary and, sometimes, secondary particles. Also, a step-by-step approach has been proposed in Monte Carlo simulations in which LET is directly computed using the true step length and the electronic energy loss at that step.

Most of the Monte Carlo simulations use a very similar method to calculate $\overline{L}_{\mathrm{d}}$, and no critical analysis has ever been done to assess the correctness of this method considering the impact of changes of important parameters involved in these calculations such as, for instance, the voxel size. The current work intends to address this critical analysis by proposing three different LET calculation methods (including the most widely used in previous publications) and assess how the variation of voxel dimensions and production threshold of secondary electrons affect the outcome of each of these methods differently, and from here elucidate if there is an unrestricted $\overline{L}_{\mathrm{d}}$ calculation method independent of variations of the mentioned parameters. These parameters are intrinsic to any condensed-history Monte Carlo simulation tool and have sufficient impact in clinical practice that makes such sensitivity analysis imperative with the objective of producing a standardization of $\overline{L}_{\mathrm{d}}$ calculations that is not affected by spurious artifacts induced by changes of the simulation setup.

The performance of each method is evaluated by comparing their calculated unrestricted $\overline{L}_{\mathrm{d}}$ values with those obtained from microdosimetric dose-mean lineal energy ($\overline{y}_{\mathrm{D}}$) calculations carried out separately and used as reference values to verify the consistency of the $\overline{L}_{\mathrm{d}}$ values obtained. All these calculations were performed in water with clinically-relevant proton beams, either pristine or spread-out Bragg peaks (SOBPs).

2. Methods

The calculations were carried out with the Geant4 (GEometry ANd Tracking) toolkit (Agostinelli *et al* 2003, Allison *et al* 2006), version 9.6.2. As $\overline{L}_{\mathrm{d}}$ and $\overline{y}_{\mathrm{D}}$ are at the core of the present calculations, we first present an overview of these two concepts.

2.1. Definitions

2.1.1. Dose average LET, $\overline{L}_{\mathrm{d}}$.

The concept of LET for therapeutic protons traveling in water is closely related to the electronic component of the linear stopping power, S_{el}, as the nuclear and radiative components are negligible at such energies (ICRU 1993). The LET is defined as the mean energy lost by charged particles, dE, travelling a distance dl through the target material (ICRU 1998 2011). The *unrestricted* LET, formally L_{∞} or, simply, L, includes the contribution of all secondary electrons in the energy lost, without restrictions applied to their initial kinetic energy; thus,

$$L = S_{\mathrm{el}}\,. \tag{1}$$

In all the simulations of this work, we calculate unrestricted LET, as done in other works (Wilkens and Oelfke 2003, Grassberger and Paganetti 2011).

LET is usually calculated as an average value, namely track average LET, $\overline{L}_{\mathrm{t}}$, or dose average LET, $\overline{L}_{\mathrm{d}}$ (ICRU 1970). In this work we focus on $\overline{L}_{\mathrm{d}}$, since it has been used to estimate the RBE of protons irradiating water and human tissue at therapeutic energies (Wilkens and Oelfke 2004, Carabe *et al* 2013). There are two equivalent methods to calculate $\overline{L}_{\mathrm{d}}$. The first considers the average along a particle track, so that $\overline{L}_{\mathrm{d}}$ is calculated as

$$\overline{L}_{\mathrm{d}} = \int L\; d(L)\;\mathrm{d}L, \tag{2}$$

where L is the unrestricted LET and $d(L)$ is the absorbed dose distribution function, i.e., $d(L)\,\mathrm{d}L$ is the fraction of the absorbed dose delivered with LET values between L and $L + \mathrm{d}L$ (ICRU 1970).

The second method considers the average as a local mean. Here, $\overline{L}_{\mathrm{d}}$ is calculated by the contribution of all particles at a certain position $\boldsymbol{x}$ of the radiation field (Wilkens and Oelfke 2003). Thus, for a voxel placed at $\boldsymbol{x}$, dose average LET is given by

$$\overline{L}_{\mathrm{d}}(\mathbf{x}) = \frac{\int_0^\infty \varphi_E(\mathbf{x})\ S^2(E)\ \mathrm{d}E}{\int_0^\infty \varphi_E(\mathbf{x})\ S(E)\ \mathrm{d}E}, \tag{3}$$

where $\phi_E(\boldsymbol{x})$ is the spectral fluence of particles entering into the voxel with a kinetic energy value between E and $E + \mathrm{d}E$, and $S(E)$ is the electronic stopping power of these particles when they pass through the target material at kinetic energy E.

2.1.2 . Dose-mean lineal energy and its relation with dose average LET. Whereas LET is often used to specify the quality of the radiation under consideration, which is intrinsically related to the energy deposition map along the particle tracks, it is not a stochastic magnitude. This stochastic nature is often important to explain the difference between the radiobiological properties of radiations with similar LET values. For this purpose, microdosimetric quantities, such as the *lineal energy*, y, are considered.

The lineal energy (ICRU 1983) is defined as the energy imparted to a delimited region of space (site or sensitive volume) by a single energy deposition event, ε_{s}, divided by the mean chord length, $\bar{l}$, of that volume,

$$y = \frac{\varepsilon_{\mathrm{s}}}{\bar{l}}\,. \tag{4}$$

The mean chord length is the mean length of randomly oriented lines crossing the sensitive biological volume (traditionally called '*site*'). For a convex site shape, $\bar{l} = 4V/A$, where V is the volume and A is the surface area of the region. Thus, for a spherical site $\bar{l} = 4R/3$, where R is the radius of the sphere. In contrast to LET, lineal energy is a stochastic and measurable quantity (Lindborg *et al* 2013).

Given the stochastic nature of particle transport through materials, the amount of energy imparted per event (i.e., single energy deposition) varies from one event to another. Thus, average values are often reported together with probability distribution functions to characterize the irradiation at a given point.

The ICRU (1983) defines the *dose-mean lineal energy*, $\bar{y}_{\mathrm{D}}$, as

$$\bar{y}_{\mathrm{D}} = \int_0^\infty y\, d(y) \quad \mathrm{d}y = \frac{\int_0^\infty y^2 f(y)\,\mathrm{d}y}{\int_0^\infty y\, f(y)\mathrm{d}y}, \tag{5}$$

where $f(y)$ and $d(y)$ are the probability and dose density distributions of lineal energy, respectively.

The relation between $\bar{y}_{\mathrm{D}}$ and $\overline{L}_{\mathrm{d}}$ is complex. Assuming a spherical site of diameter d irradiated with protons with considerably longer residual range, the following expression was demonstrated (Kellerer 1985):

$$\bar{y}_{\mathrm{D}} = \frac{9}{8}\overline{L}_{\mathrm{d}} + \frac{3\delta_2}{2\mathrm{d}}, \tag{6}$$

where δ_2 represents the weighted average of the energy imparted per collision of the traversing charged particle including all the energy deposits made by the correlated secondary electrons,

ε_c. Let $f_c(\varepsilon_c)$ be the probability density of ε_c. Assuming that the energy transferred per collision equals the energy actually imparted (i.e., no effluence of δ-rays released within the sensitive volume) and free electron model, roughly $f_c\,(\varepsilon_c) \equiv f_{c,\mathrm{free}}\,(\varepsilon_c) = k\,/\,\varepsilon_c^2$, where k is a normalization constant. Under these assumptions (Kellerer 1985), δ_2 is obtained from

$$\delta_2 = \frac{\int \varepsilon_c^2\, f_{c,\mathrm{free}}\,(\varepsilon_c)\;\mathrm{d}\varepsilon_c}{\int \varepsilon_c\, f_{c,\mathrm{free}}\,(\varepsilon_c)\,\mathrm{d}\varepsilon_c} \approx \frac{\varepsilon_{\max}}{2\ln\left(\varepsilon_{\max}\,/\,I\right)}, \tag{7}$$

where $\varepsilon_{\max}$ is the maximum energy loss in one collision (approximately equal to the maximum energy transferred by a heavy particle to a free electron at rest) and I is the mean ionization potential of the medium; for water, the I-value is 78 eV according to ICRU (2005). If the range of the δ-rays produced by the traversing charged particle is expected to be larger than the site diameter, then the calculation of δ_2 has to be corrected due to the effluence of δ-rays released within the site, since the probability distribution of energy imparted in single collisions becomes different from $f_{c,\mathrm{free}}(\varepsilon_c)$, as discussed by Kellerer (1985). The result is that the effective value of $\varepsilon_{\max}$ is influenced by the site diameter. Roughly, this effective $\varepsilon_{\max}$ can be approximated to an effective energy value, E_d, which corresponds to the energy of an electron with range similar or slightly smaller than the diameter of the site (Kellerer 1985). Thus,

$$\delta_2 \approx \frac{E_\mathrm{d}}{2\ln\left(E_\mathrm{d}\,/\,I\right)}\,. \tag{8}$$

In this work, we focus on comparing different $\overline{L}_\mathrm{d}$ calculation methods carried out for primary protons in water irradiated by therapeutic beams. The values obtained are compared with $\overline{L}_\mathrm{d}$ values estimated from $\overline{y}_\mathrm{D}$ calculations as consistency verification. We consider only primary protons in order to do straightforward comparisons between the different $\overline{L}_\mathrm{d}$ Monte Carlo calculation methodologies. In the subsequent subsections we will: (i) explain the geometries used to calculate $\overline{L}_\mathrm{d}$ and $\overline{y}_\mathrm{D}$ with Monte Carlo simulations, (ii) show the different Monte Carlo methodologies to calculate $\overline{L}_\mathrm{d}$, and (iii) compare the $\overline{L}_\mathrm{d}$ values determined from $\overline{y}_\mathrm{D}$ calculations (6) with the $\overline{L}_\mathrm{d}$ values calculated at the same depth in water in order to validate the most consistent $\overline{L}_\mathrm{d}$ calculation method.

2.2. Setups used in the Monte Carlo simulations

2.2.1. Dose average LET, $\overline{L}_\mathrm{d}$. The geometry used for dose and $\overline{L}_\mathrm{d}$ calculations consisted of a water tank in which cylindrical voxels were defined as depicted in figure 1 for scoring purposes. The transversal width and thickness along the central axis of the voxels were set by the parameters Δr and Δz, respectively. Δr defined the distance between voxel boundaries along transversal axes, so that central voxels had a diameter of Δr and off-axis ones had a transversal width of Δr. Δz defined the voxel thickness along the water tank central axis. The value of Δr was varied between 0.5 and 5.0 mm, whereas Δz was varied between 0.2 and 2.0 mm in order to consider clinically relevant voxel dimensions. Voxels were defined up to a 10 cm transversal distance from the central axis and at a 30 cm depth. Water material was simulated with *G4_WATER*, taken from the Geant4 NIST database.

We used the set of physics models (also referred to as 'physics list') recommended for the simulation of therapeutic proton beams with Geant4 (Romano *et al* 2014). Electromagnetic interactions were simulated with *G4EmStandardPhysics_option3* physics list builder, which implements a condensed-history algorithm based on the Bethe-Bloch restricted energy loss formula for proton transportation; further details are provided in the Geant4

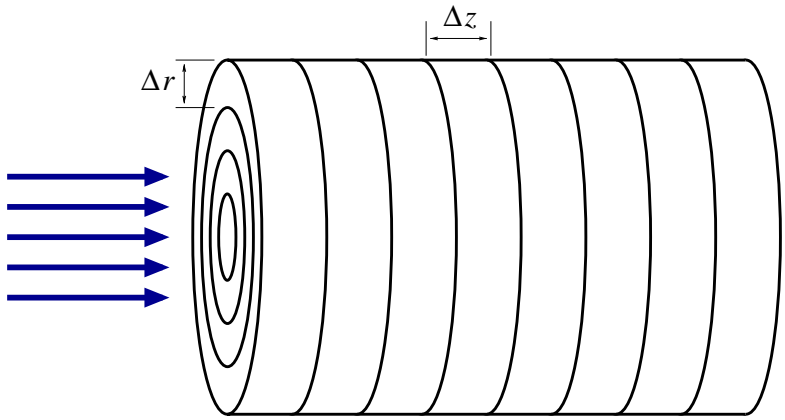

Figure 1. Scheme of the cylindrical geometry used for the calculation of dose average LET in water. The beam enters from the left. Δz sets the voxel thickness along the beam axis. Δr sets the distance between voxel boundaries along the transverse axes.

Physics Reference Manual (GEANT4, chapter 12). Hadronic interactions were reproduced with models implemented in the *QGSP_BIC_HP* physics list, in which Geant4 native pre-equilibrium and de-excitation models are used as low energy stages of the Binary Cascade model (Folger *et al* 2004, Quesada *et al* 2011) for protons, neutrons and ions. As for the tracking of secondary particles, the production cut value was varied between 0.05–0.20 mm for electrons, photons and positrons. Thus, secondary particles (e.g., δ-rays) were explicitly produced only if their initial kinetic energy was such that the expected range in the medium (water) was larger than the production cut value. Otherwise, the secondary particle was not explicitly tracked, its kinetic energy considered as deposited along the step done by the primary particle.

2.2.2. Dose-mean lineal energy, $\bar{y}_D$. Microdosimetry calculations were carried out with a simple simulation which geometry consisted of a spherical sensitive volume contained within the world volume, as shown in figure 2. The aim of these simulations was to calculate $\bar{y}_D$ *values at certain depths in the water tank setup (see previous section) to estimate* $\overline{L}_d$ values according to (6). To do this, we followed the approach described below:

- Although Geant4 includes the Geant4-DNA package (Incerti *et al* 2010), which makes it possible to carry out track-structure simulations with the Geant4 toolkit, we decided to simulate δ-ray transport with models included in the *G4EmPenelopePhysics* physics list, which includes transport models based on the version 2008 of the PENELOPE code (Salvat *et al* 2009). Despite following a condensed-history approach, this physics list can produce δ-rays down to an initial kinetic energy of 100 eV (which corresponds to an electron range of roughly 0.6 μm in water), thus providing reliable results at a scale of ~10 μm. In fact, Burigo *et al* (2014) recently showed a good agreement between *G4EmPenelopePhysics* and Geant4-DNA for a wall-less tissue equivalent proportional counter (TEPC) simulating a tissue volume of 0.72 µm. For these reasons, we set a scoring sphere radius, R_c, of 5 μm and used *G4EmPenelopePhysics*, for the sake of achieving an acceptable computing efficiency with a simple geometry. As for hadronic interactions, we kept *QGSP_BIC_HP*, mentioned in the previous section.

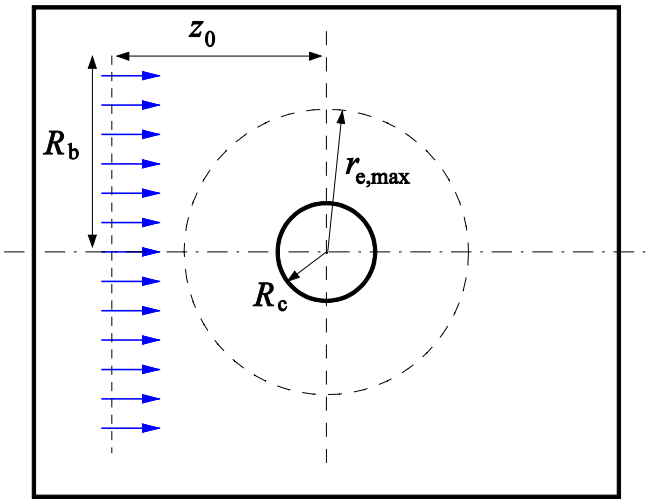

Figure 2. Scheme of the geometry used for microdosimetry simulations (2D projection). A spherical volume of radius $R_c = 5\,\mu m$ is placed for scoring purposes within a larger water volume. The primary proton beam (arrows) has a circular shape of radius R_b and is placed at a distance z_0 from the center of the cavity. The maximum range of δ-rays, $r_{e,max}$, is also illustrated.

- If the scoring volume were simulated within the water tank setup, we would need to simulate a huge number of primary protons in order to achieve good energy deposition statistics within the sphere; thus, we defined a microscopic simulation setup in which the spherical sensitive volume was placed at the center of a world volume of 5 mm sides. To define the energy spectrum of the proton beam which irradiated the sensitive volume, we previously ran a simulation of the water tank setup which created a phase-space file in IAEA format (Cortés-Giraldo *et al* 2012) at the depth of interest, from which the energy spectrum was extracted and stored into a ROOT histogram. The histogram was then used to produce the energy spectrum of the proton beam in this microscopic setup, so that the sensitive volume was virtually irradiated at the depth of the phase-space plane.
- In order to ensure that the sensitive volume was irradiated uniformly and that all indirect events were simulated (i.e., events where the energy imparted to the sensitive volume is only due to δ-rays), we estimated the maximum range of δ-rays produced by the beam, $r_{e,max}$. To do this, we obtained the maximum energy value of the proton beam spectrum and calculated the maximum kinetic energy transferred to a δ-ray, from which $r_{e,max}$ was estimated by means of NIST's ESTAR program (Berger *et al* 2005), based on tables published by ICRU (1984). Thus, the spatial distribution of the proton beam was a uniform circle with a radius, R_b, about $10\,\mu m$ larger than $r_{e,max}$; also, the proton beam was produced at a distance to the center of the site, z_0, about $10\,\mu m$ larger than $r_{e,max}$, as shown in figure 2.

We point out that the aim of these microscopic calculations is just to obtain $\bar{y}_D$ *values for a microscopic sensitive volume placed at several depths in water in order to estimate* $\bar{L}_d$ according to (6). These simulations do not aim to perform microdosimetry calculations with track structure analysis purposes, as done in other works with 10 nm target volumes (Francis *et al* 2012, Lindborg *et al* 2013). Nevertheless, figure 3 shows the $y{\cdot}d(y)$ distributions calculated with Geant4-DNA and *G4EmPenelopePhysics* with a uniform proton beam where its energy spectrum

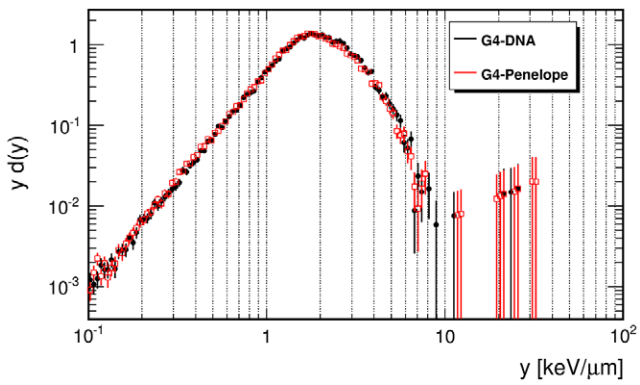

Figure 3. $y{\cdot}d(y)$ distributions obtained with Geant4-DNA (filled circles) and *G4EmPenelopePhysics* (open circles) for a spherical sensitive volume (5 μm radius) uniformly irradiated with protons. The energy distribution of the beam was previously calculated at a 16.5 cm depth in a water tank irradiated with a 160 MeV proton beam, which corresponds to a proton mean energy of approximately 35.1 MeV. Statistical uncertainty (1σ) is shown with error bars.

was calculated at 16.5 cm depth in water (mean energy of 35.1 MeV, approximately). The agreement is remarkable and justifies the usage of *G4EmPenelopePhysics* in our simulations.

In order to keep a coherent comparison with the $\overline{L}_{\mathrm{d}}$ values calculated with the water tank setup, we only scored primary protons and their δ-rays for the calculation of $\overline{y}_{\mathrm{D}}$, i.e., the energy imparted due to fragments produced by nuclear reactions was not taken into account. To derive $\overline{L}_{\mathrm{d}}$ from $\overline{y}_{\mathrm{D}}$ by means of (6), we estimated E_d in (8) from $\varepsilon_{\mathrm{c}}\,\mathrm{f}_c(\varepsilon_{\mathrm{c}})$ and $\varepsilon_{\mathrm{c}}^2\,\mathrm{f}_c(\varepsilon_{\mathrm{c}})$ calculations (see appendix). This was done because of the 100 eV production threshold mentioned above, which essentially cuts $\mathrm{f}_c(\varepsilon_{\mathrm{c}})$ below this value; therefore, we could not obtain any information of $\mathrm{f}_c(\varepsilon_{\mathrm{c}})$ below this threshold. An example is shown in figure 4, which presents $\varepsilon_{\mathrm{c}}^2\,\mathrm{f}_c(\varepsilon_{\mathrm{c}})$ calculated with the site irradiated by protons where its energy distribution was previously calculated at 15 cm depth in a water tank irradiated with a 160 MeV proton beam. Thus, in order to overcome this limitation we decided to estimate the value of E_{d} as indicated in the appendix.

The calculation of the energy imparted within the sensitive volume per proton single collision, ε_{c}, was done in our Geant4 application by scoring separately each shower started by a secondary electron set in motion in the site by a primary proton. For this purpose, we coded a sensitive detector class in which the track ID of each secondary electron released due to primary proton interactions was used to tag each δ-ray shower. Thus, the energy deposited in the site by each δ-ray shower, including δ-rays created by further collisions of the electron originating the shower, could be scored independently of each other.

2.3. Dose average LET calculation methods

$\overline{L}_{\mathrm{d}}$ can be calculated from definitions (2)–(3) in Monte Carlo simulations in an event-by-event basis as

$$\overline{L}_{\mathrm{d}} = \frac{\sum_n \left(\frac{\mathrm{d}E}{\mathrm{d}l}\right)\,\mathrm{d}E}{\sum_n \mathrm{d}E}, \tag{9}$$

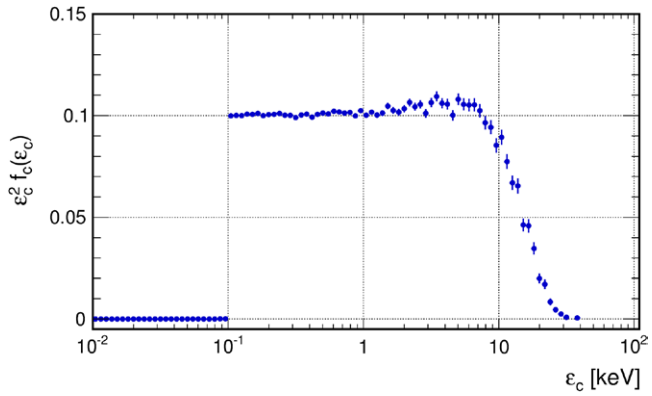

Figure 4. Monte Carlo calculation of $\varepsilon_c^2\, f_c(\varepsilon_c)$ distribution for a spherical sensitive volume (5 μm radius) irradiated with protons. The energy distribution of the beam was previously calculated at a 15.0 cm depth in a water tank irradiated with a 160 MeV proton beam, which corresponds to a proton mean energy of approximately 55 MeV. Statistical uncertainty (1σ) is shown with error bars.

where n is the event index, dE is the energy lost and dl the track length for each event. Equation (9) does not specify how (dE / dl) dE is computed within each particular event. Thus, since the number of steps needed to transport each proton along a given voxel varies from each other, the numerator of (9) can be computed in a step-by-step basis or, as another approach, the numerator and denominator of the quotient (dE / dl) can be computed separately for all steps done within a given voxel through prior multiplication by the energy deposition in the voxel.

Let us represent the event index with n and the step index of the primary proton simulated at that event with s. If we consider that the number of steps performed to transport the primary proton along the voxel at the event n is S_n, and the total number of events simulated is N, the step-by-step computation of (9) becomes

$$\overline{L}_{\mathrm{d}} = \frac{\sum_{n=1}^{N} \sum_{s=1}^{S_n} \omega_n \frac{\varepsilon_{sn}^2}{l_{sn}}}{\sum_{n=1}^{N} \sum_{s=1}^{S_n} \omega_n\, \varepsilon_{sn}}, \tag{10}$$

where l_{sn} and ε_{sn} are, respectively, the length and the electronic energy loss by the primary proton during the step s of event n, and ω_n is the statistical weight of the primary proton. Since we are interested in calculating unrestricted $\overline{L}_{\mathrm{d}}$, ε_{sn} is calculated as the energy deposited by the primary proton along the step (i.e., the continuous part of the energy deposition due to the passage of the primary proton) plus the kinetic energy of the δ-rays released in the medium in that step.

Alternatively, we can compute separately the electronic energy loss ε_{sn} and step length l_{sn} for all the steps done by a primary proton within a given voxel through prior calculation of the LET and multiplication by the weighting factor of the average. This gives the following scoring of $\overline{L}_{\mathrm{d}}$:

$$\overline{L}_{\mathrm{d}} = \frac{\sum_{n=1}^{N}\left[\omega_n \frac{\left(\sum_{s=1}^{S_n} \varepsilon_{sn}\right)^2}{\sum_{s=1}^{S_n} l_{sn}}\right]}{\sum_{n=1}^{N}\left[\omega_n \sum_{s=1}^{S_n} \varepsilon_{sn}\right]}. \tag{11}$$

Clearly, (10) and (11) only become equivalent if all the primary protons cross the voxel in only one step, which for instance happens when δ-rays are not explicitly tracked in the simulation; this means in Geant4 there is a large value of the production threshold of secondary particles. In any other case, (10) and (11) can become significantly different since each simulation step AQ4 finishes whenever a δ-ray is produced.

A variation of (10) was also implemented as the third $\overline{L}_{\mathrm{d}}$ calculation method. Instead of computing the LET as the quotient between the actual electronic energy loss and step length computed during the simulation, we calculated the LET of the step, L_{sn}, as the corresponding *mean* energy loss per unit path length in the material according to the proton kinetic energy at the step. In our code, L_{sn} was obtained with the method *ComputeElectronicDEDX()* of *G4EmCalculator* class. This method can be called at each step and calculates the LET from electronic stopping power tables built at the beginning of the simulation, once particle type, kinetic energy and material are provided. The kinetic energy was the arithmetic mean between the values at pre- and post-step points. Further, L_{sn} was calculated only for steps terminated only by an electromagnetic interaction (such as δ-ray production by ionization) or a boundary crossing, since other kinds of interactions (e.g., inelastic hadronic) may completely lose the identity of the track. Thus, the average of L_{sn} weighted by the electronic energy loss (ε_{sn}) computed at that step yields

$$\overline{L}_{\mathrm{d}} = \frac{\sum_{n=1}^{N}\sum_{s=1}^{S_n} \omega_n L_{sn} \varepsilon_{sn}}{\sum_{n=1}^{N}\sum_{s=1}^{S_n} \omega_n \varepsilon_{sn}}. \tag{12}$$

For the sake of simplicity, in references hereafter we refer to the methods described in (10)–(12) as 'A', 'B' and 'C', respectively.

2.4. Validation of the $\overline{L}_{\mathrm{d}}$ calculation methodologies

Two proton beam types were considered. First, the water tank was irradiated by a 160 MeV proton beam with an energy spread σ_E = 1.04 MeV; the beam profile was modeled as a 2D Gaussian with σ = 8.9 mm in both transversal axes. $\overline{L}_{\mathrm{d}}$ was calculated with (10)–(12) within the water tank along the beam axis. Microdosimetry $\overline{y}_{\mathrm{D}}$ values were calculated for proton energy spectra taken at several depths and the corresponding $\overline{L}_{\mathrm{d}}$ value, estimated by means of (6), was compared with those calculated at the same depths with the scoring methods described in (10)–(12).

Second, broad beams were considered to produce arbitrary SOBPs. In this case, the beam profile was uniform along transversal directions, circular shape and radius of 3.0 cm. The mean energy, spectral width and weight of each pristine Bragg peak were taken from pencil beam scanning calculations done with the treatment planning system used at the University

of Pennsylvania (Eclipse, Varian). Normal incidence on the water tank was considered, for simplicity, since this work aims to compare various Monte Carlo calculation methods of $\overline{L}_{\mathrm{d}}$ and not to reproduce accurately the dose or $\overline{L}_{\mathrm{d}}$ maps.

3. Results

Figure 5 shows $\overline{L}_{\mathrm{d}}$ values calculated with methods 'A' (top), 'B' (middle) and 'C' (bottom) for a 160 MeV proton beam of Gaussian profile and energy spectrum ($\sigma_x = \sigma_y = 8.9$ mm; $\sigma_E = 1.04$ MeV); 10^8 primary protons (events) were simulated. The production cut of secondary particles was 0.05 mm. Scoring was done along the central axis of a voxel grid with $\Delta r = 5.0$ mm and Δz value between 0.2 and 2.0 mm; the $\overline{L}_{\mathrm{d}}$ value calculated for primary proton tracks is reported at the central point of each voxel. Steps with lengths smaller than 2 nm (roughly the width of a DNA molecule) were not taken into account to ensure numerical stability. These calculations are compared with the $\overline{L}_{\mathrm{d}}$ values obtained from $\overline{y}_{\mathrm{D}}$ microdosimetry calculations carried out by irradiating a 5 μm spherical volume with protons of the same energy spectrum as that obtained in the water tank at the depth considered. Table 1 shows, for several depths, the calculated $\overline{y}_{\mathrm{D}}$ (with 1σ statistical uncertainties), E_{d} and δ_2 values estimated from the probability density of energy imparted per single collision (see previous section and appendix), and the corresponding $\overline{L}_{\mathrm{d}}$ calculated from (8) together with their uncertainties. Since (6) is valid only if the proton residual range is considerably larger than the site diameter, we only report calculations up to ~5 mm upstream from the Bragg peak position.

Clearly, there is a significant impact on the calculated $\overline{L}_{\mathrm{d}}$ values not only due to the method used but also due to the voxel thickness, Δz. Moreover, the differences shown around the Bragg peak region (depth larger than ~1 cm upstream from the depth of the maximum dose) are of a different nature than those found at the entrance and plateau region (up to ~15 cm depth).

Method 'A' shows a significant variation at the entrance and dose plateau region (roughly up to 15 cm depth) towards higher $\overline{L}_{\mathrm{d}}$ values as Δz becomes smaller. However, these calculations give stable results around the Bragg peak region (depths larger than 16 cm) against changes of the voxel thickness, Δz, which is the expected result since the LET distribution at a given depth should not vary because of the voxel dimensions used for scoring. Method 'B' performs better than method 'A' at the dose plateau region, since it shows smaller systematic variations and a better agreement with the $\overline{L}_{\mathrm{d}}$ values estimated from the microdosimetry calculations. However, method 'B' shows a clear systematic variation beyond the Bragg peak position. Method 'C' shows better performance than the others, since no variations are observed due to changes in Δz and also presents a good agreement with respect to $\overline{L}_{\mathrm{d}}$ obtained from microdosimetry.

The origin of the systematic variation observed in the $\overline{L}_{\mathrm{d}}$ value obtained at the dose plateau region with method 'A' is shown in figure 6. The upper histogram presents the electronic energy loss per primary proton step, ε_s, *versus* the step length, l_s, within a voxel placed at the central axis at 4.0 cm depth, $\Delta z = 0.5$ mm, normalized to the total number of steps done by primary protons inside this voxel. As expected, most step lengths are roughly equal to Δz. Also, the LET of bins with the highest number of counts is between 0.1 and 1.0 keV μm^{-1}, compatible with the LET of a proton with energy equal to the mean of the energy spectrum (137.8 MeV, which LET in water is 0.58 keV μm^{-1}). However, this histogram also presents a horizontal tail which includes bins associated with higher LET values. This tail appears due to steps which have been terminated by the condensed-history algorithm to generate explicitly a δ-ray above the production threshold of secondary particles, as demonstrated at the middle

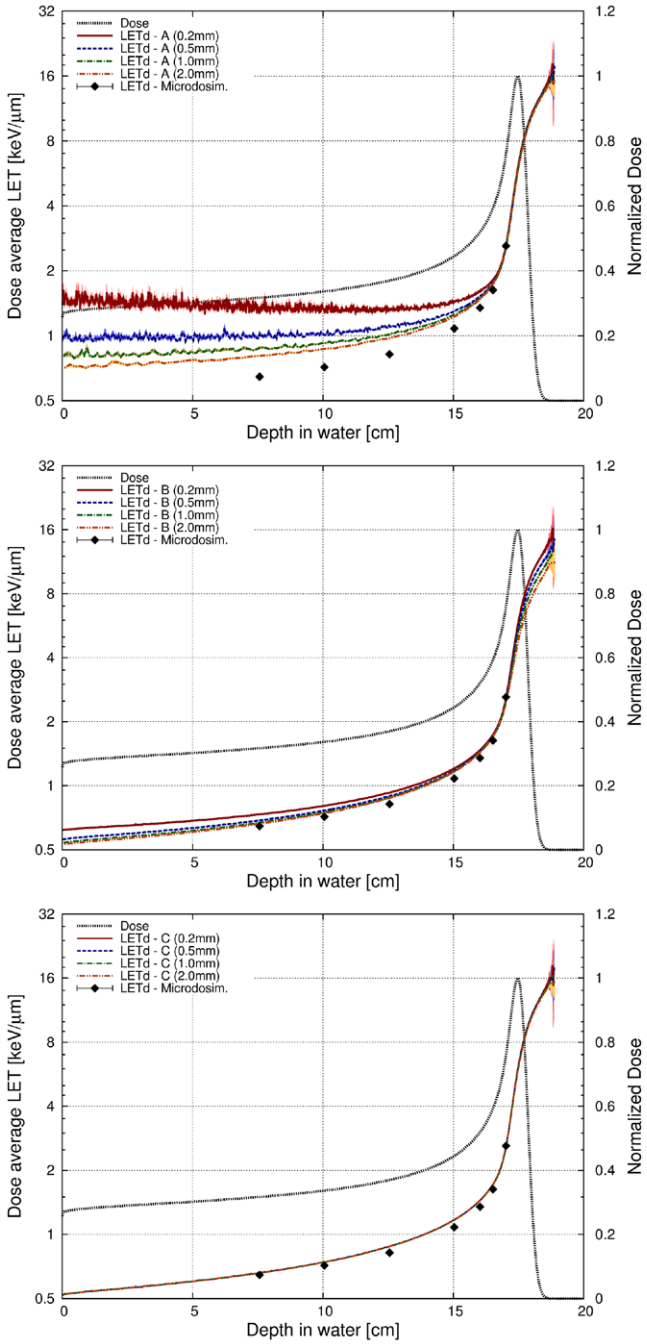

Figure 5. Dose average LET calculated with methods 'A' (top), 'B' (middle) and 'C' (bottom) along the central axis of a water tank irradiated by a 160 MeV proton beam; scoring voxel thicknesses (Δz) of 0.2 mm (solid lines), 0.5 mm (dashed), 1.0 mm (dot dashed) and 2.0 mm (double dot dashed) were considered; statistical uncertainty (1σ) is reported with shadow bands visible. Diamonds show the dose average LET values obtained from dose-mean lineal energy ($\bar{y}_D$) calculations in a water spherical volume of 5 μm radius (see table 1); statistical uncertainties (1σ) are contained within the symbol size. Depth dose profile normalized to maximum is shown with a dotted line. Dose average LET is reported only for voxels with dose deposition greater than 0.1% of maximum.

Table 1. Results obtained in a water spherical site (5 μm radius) virtually irradiated by a 160 MeV beam at the reported depth in a water tank: Dose-mean lineal energy ($\bar{y}_D$), estimated E_d, corresponding δ_2 calculated with (8), and $\bar{L}_d$ obtained with (6).

Depth (cm)	$\bar{y}_D$ (keV μm^{-1})	E_d (keV)	δ_2 (keV)	$\bar{L}_d$ (keV μm^{-1})
7.5	0.959(7)	16.6(2)	1.55(11)	0.646(15)
10.0	1.033(7)	16.2(2)	1.52(10)	0.716(15)
12.5	1.154(7)	16.4(2)	1.53(11)	0.821(15)
15.0	1.446(5)	16.4(2)	1.53(11)	1.081(15)
16.0	1.745(6)	16.3(2)	1.53(10)	1.348(15)
16.5	2.063(12)	16.2(2)	1.52(10)	1.63(2)
17.0	3.16(2)	15.4(2)	1.46(10)	2.61(2)

plot of this figure, which presents only steps of this type. The tail appears because the initial kinetic energy of any δ-ray explicitly tracked in the simulation is always greater than the energy threshold that corresponds to the production cut value. Thus, the electronic energy loss of the primary proton in steps terminated by an ionization process which explicitly produces a δ-ray above the energy threshold must always be greater than such an energy value due to energy conservation. However, the proton step length rarely becomes larger than Δz, since the step is finished when the proton reaches a volume boundary. As a consequence, the LET calculated at such a step according to method 'A' may become spuriously high if the step length remains short due to voxel boundary crossing. This introduces spurious high LET terms into the weighted average which produces the systematic bias of higher LET values for smaller Δz observed for method 'A' in figure 5. In these calculations, the production cut of secondary electrons was 0.05 mm, which corresponds to an initial kinetic energy threshold of 0.057 MeV in water. Thus, the minimum possible value of the electronic energy loss (ε_s) of the proton at such steps is roughly 0.06 MeV which is independent of the step length, as observed in the histogram. The lower histogram of figure 6, presents the data used to calculate $\bar{L}_d$at the same voxel according to method 'B' (11). It shows the electronic energy loss of primary protons along the trajectory described within the voxel *versus* the trajectory length; in other words, ε_s and l_s are summed separately over all the simulation steps done by each primary proton within the voxel. This histogram is normalized to the number of primary protons reaching the voxel. Here, it is clearly observed that the high LET bins due to steps emitting secondary electrons do not appear, explaining why method 'A' produces larger $\bar{L}_d$ values than 'B' at the entrance/plateau region. This can be deduced by analyzing the terms constituting the weighted average in both methods (10) and (11). In method 'A', each term is produced by one step done during the proton transport, whereas in method 'B' each term is created by grouping the energy losses and lengths of all the steps done for the proton transport within the voxel. Thus, the contribution of the steps with high LET associated is more significant in method 'A', where each constitutes an individual term at the numerator of the weighted average (10), than in method 'B', where these δ-ray-emitting steps are grouped with at least another step (that one needed to complete the proton trajectory within the voxel after the emission of the δ-ray, as shown in figure 7) to constitute one of the terms of the weighted average (11).

We would like to point out that the impact of the high LET tail on calculation method 'A' becomes lower as the depth increases. This occurs because the kinetic energy decreases as the proton beam penetrates into the water tank, and so does the maximum kinetic energy transferred to δ-rays. Consequently, the probability of emitting δ-rays with an expected range above the production threshold (0.05 mm) decreases, thus the number of δ-rays tracked in

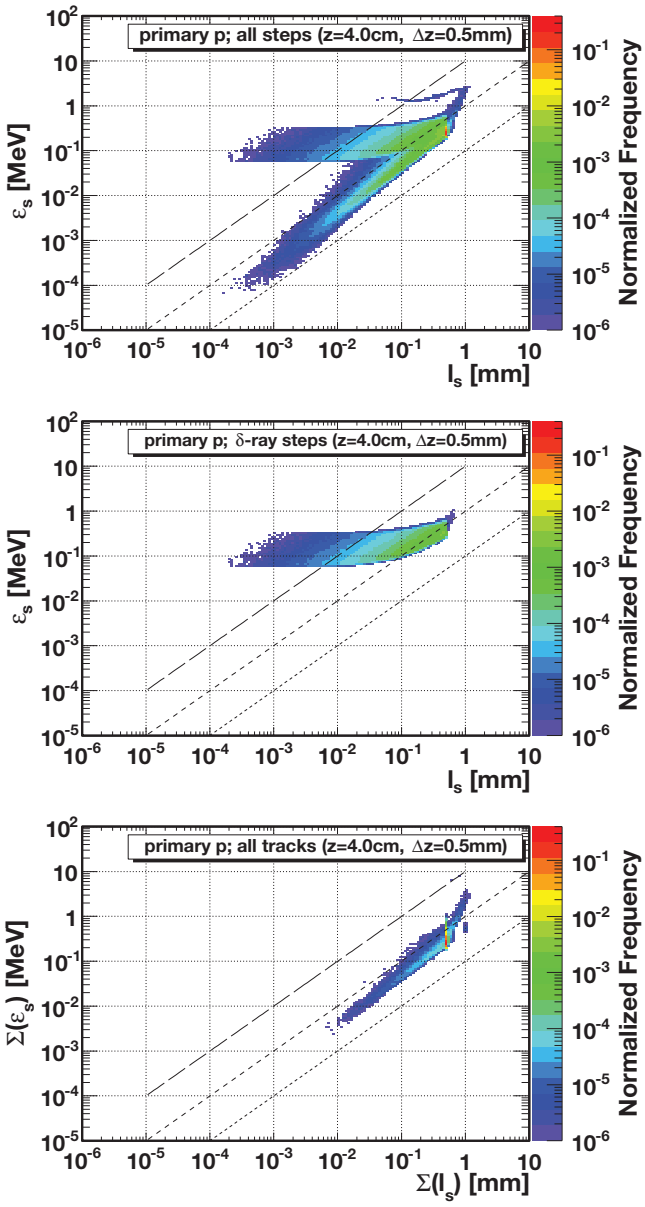

Figure 6. (Top) 2D histogram showing the correlation between the energy loss by primary protons due to electronic collisions per step (ε_s) and the step length (l_s) for a voxel placed at a 4.0 cm depth (Δz = 0.5 mm), with a160 MeV proton beam. Diagonal lines show iso-LET curves for 0.1 keV μm^{-1} (short dashed), 1.0 keV μm^{-1} (dashed) and 10 keV μm^{-1} (long dashed). Frequency normalized to the total number of steps registered within the voxel is reported. (Middle) Subset of upper plot, reporting only steps creating secondary electrons explicitly. (Bottom) Data used in method 'B' for the same voxel: Electronic energy loss by each primary proton along the trajectory described inside the voxel *versus* the corresponding trajectory length at the same voxel. Frequency is normalized to the total number of tracks in this case.

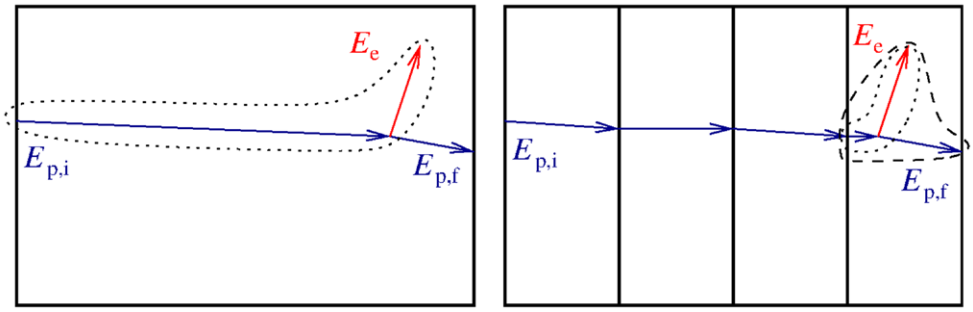

Figure 7. Schematic example of the same physical situation simulated with large (left) or small voxels (right). In both cases, a proton (simulation steps represented by blue arrows) loses the same amount of energy, $E_{p,i} - E_{p,f}$, along its path and emits at the same point a δ-ray (red arrow) with initial kinetic energy E_e above the energy threshold for secondary electrons. The dotted line indicates the step which produces the δ-ray; note the step length difference between both plots. The dashed line (right plot) marks the proton steps used to calculate the unrestricted LET of the voxel where the δ-ray is emitted according to method 'B'.

the simulation decreases as the depth increases. Therefore, the bias observed for method 'A' becomes lower as the depth (beam energy) increases (decreases).

There is a similar occurrence when comparing $\overline{L}_d$ distributions obtained with different values of the production threshold of secondary particles, as shown in figure 8 for production cut values of 0.05, 0.10 and 0.20 mm with a voxel thickness (Δz) of 0.05 mm. As the production threshold value increases, the bias introduced by scoring method 'A' decreases because the probability of explicit secondary electron emission decreases and so does the influence of δ-ray-emitting steps into the weighted average (10). This trend is in accordance with the fact that scoring method 'A' should converge to method 'B' if the production threshold value becomes large enough so that no δ-rays are explicitly transported during the simulation. Methods 'B' and 'C' showed no significant variations against changes of the production threshold. This is the expected behavior of scoring method 'C', since it only depends on the kinetic energy of the proton. As for method 'B', this is probably explained because the contribution of δ-ray-emitting steps is not as important as in method 'A', as discussed above.

Figure 9 aims at explaining the variations observed in the $\overline{L}_d$ values calculated with method 'B' at the dose plateau region. It shows the LET distribution of primary protons reaching a voxel placed along the central axis at a 4.0 cm depth with thickness Δz of 0.2 mm, 0.5 mm and 2.0 mm, respectively. LET is calculated as the electronic energy loss along the trajectory described within the voxel over the trajectory length. Histograms are normalized to the number of primary protons reaching the voxel. The maximum difference between the mean values of the distributions is less than 0.25%, which is due to the fact that the proton LET varies as it travels through the water and that the voxel limits change for different voxel sizes although the geometric center remains at the same place. However, the variance of the distribution becomes larger for smaller Δz values; in other words, the second moment of the LET distribution increases for decreasing Δz and therefore the $\overline{L}_d$ value calculated with method 'B' becomes larger for smaller Δz, as observed previously in figure 5.

Figure 10 shows the origin of the systematic deviation observed for the $\overline{L}_d$ calculation method 'B' at the Bragg peak. Thus, the LET is calculated as the quotient between the electronic energy loss of each primary proton over the trajectory length within a given voxel. In

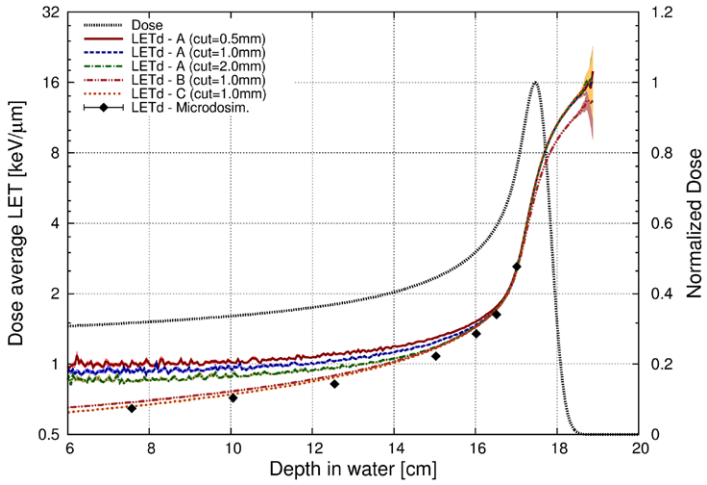

Figure 8. The same as figure 5 for dose average LET calculations obtained with production cut values of 0.05, 0.10 and 0.20 mm using scoring methods 'A', 'B' and 'C'. The voxel thickness (Δz) was 0.5 mm. Methods 'B' and 'C' are reported with only one curve since they did not show significant variations between different production cut values.

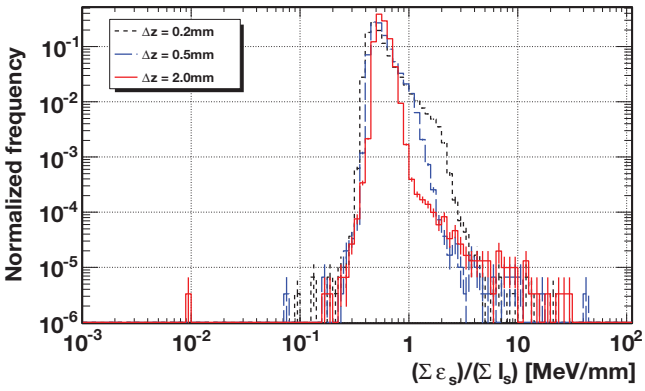

Figure 9. LET distributions of primary protons computed with method 'B' (11) for a 160 MeV beam in a voxel placed at a 4.0 cm depth, size Δz of 0.2 mm (short-dashed histogram), 0.5 mm (long dashed) and 2.0 mm (solid). The mean value of each histogram is 0.5750(1) keV μm^{-1}, 0.5751(1) keV μm^{-1} and 0.5763(1) keV μm^{-1}, respectively. Error bars show 1σ statistical uncertainties.

these plots, the LET is represented *versus* the corresponding electronic energy loss and we report calculations obtained for a voxel placed at the central axis, with 17.8 cm depth (about 0.3 cm downstream from the Bragg peak). The plots correspond to a voxel thickness (Δz) of 0.2 mm (top), 0.5 mm (middle) and 2.0 mm (bottom), respectively. They clearly show that bins are filled around two lines that cross at a given point. The lower diagonal line corresponds to primary protons completely crossing the voxel, whereas the upper arched line is filled by primary protons absorbed within the voxel (since the electronic energy loss decreases for increasing

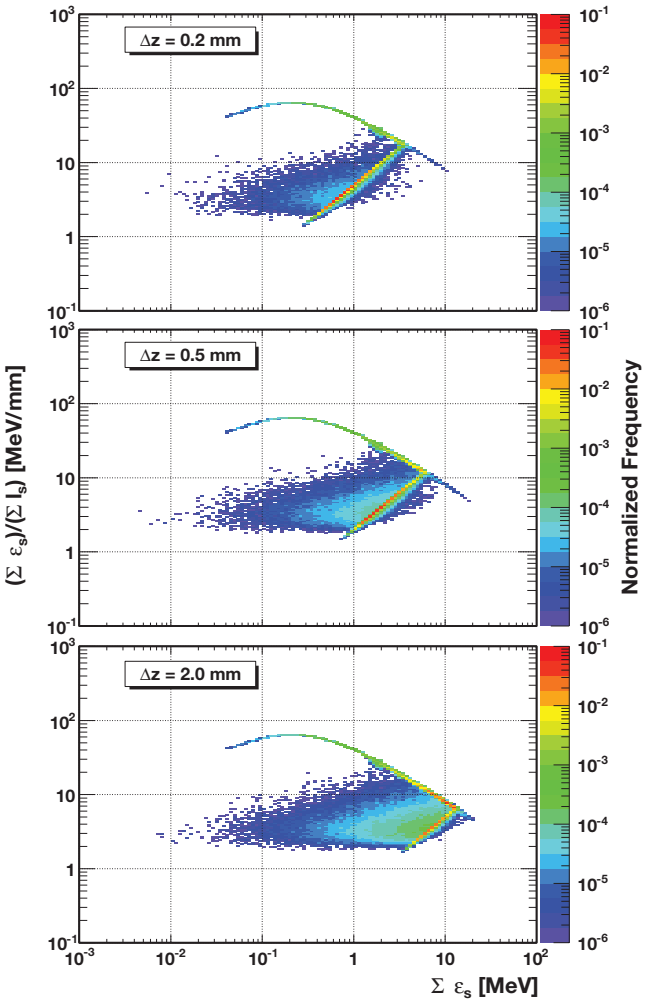

Figure 10. LET computed with method 'B' (11) *versus* the corresponding electronic energy loss for each primary proton track of a 160 MeV proton beam at a voxel placed at the central axis, at a 17.8 cm depth. The voxel thickness (Δz) is 0.2 mm (top), 0.5 mm (middle) and 2.0 mm (bottom), respectively. Frequency normalized to the number of scoring protons is presented.

LET, the track length has to be smaller). According to (11), the bins around the crossing point have the largest weighting factor values of $\overline{L}_{\mathrm{d}}$ (presented at x axis). It is observed that the value of the crossing point on the y axis increases for decreasing Δz. Thus, the LET of bins with the greatest weighting factor becomes larger as Δz decreases and consequently $\overline{L}_{\mathrm{d}}$ becomes larger for smaller Δz. In this particular case, the $\overline{L}_{\mathrm{d}}$ value was 6.6 keV μm^{-1}, 7.8 keV μm^{-1} and 8.4 keV μm^{-1} for a Δz value of 2.0 mm, 0.5 mm and 0.2 mm, respectively. These deviations are a consequence of the rapid variation of the LET at the end of the proton trajectory; thus, it is expected that the $\overline{L}_{\mathrm{d}}$ value obtained with two voxels of different size, centered at the same point, varies since the interval in which the LET is averaged changes.

In contrast, the voxel thickness did not have a significant impact on the calculation of $\overline{L}_{\mathrm{d}}$ with methods 'A' and 'C'. In method 'A' (10), the average is done over LET values calculated

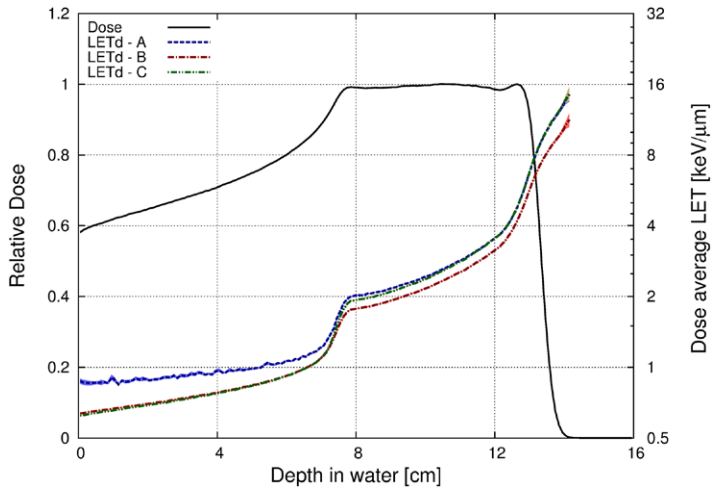

Figure 11. SOBP for a medulloblastoma treatment (solid line, range of 13.0 cm, modulation width of 5.9 cm) and dose average LET calculated with methods 'A' (dashed), 'B' (dot dashed) and 'C' (double dot dashed), respectively. Statistical uncertainties (1σ) are shown with shadow bands.

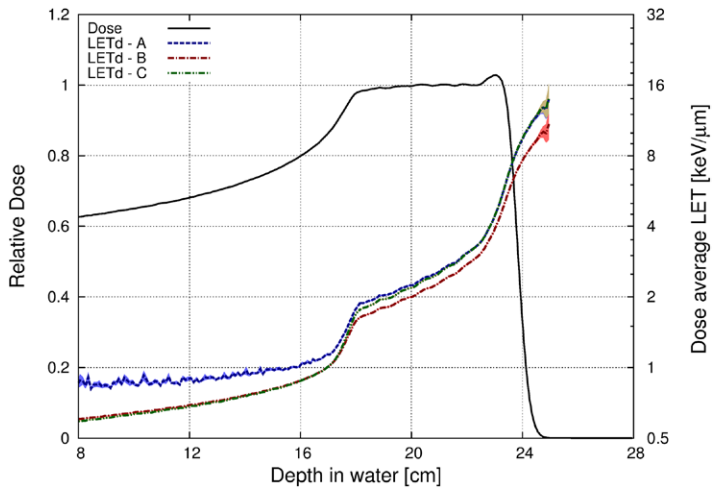

Figure 12. The same as figure 11 for a prostate case; SOBP range of 23.5 cm, modulation width of 6.2 cm.

for each individual step. As mentioned previously, few secondary electrons are explicitly simulated at the Bragg peak region (the expected range is generally below the production cut) and hence the effect discussed previously in figure 6 is not significant here. In method 'C' (12), the LET is calculated at each step by interpolation of electronic stopping data tables according to the proton kinetic energy and traversing material; thus, neither voxel thickness nor δ-ray production has any effect on the calculated value of $\overline{L}_{\mathrm{d}}$ by means of method 'C'.

Figures 11–13 show the $\overline{L}_{\mathrm{d}}$ values calculated along the central axis for three SOBPs: A low energy one, defined for the treatment of a medulloblastoma (figure 11, with a range and

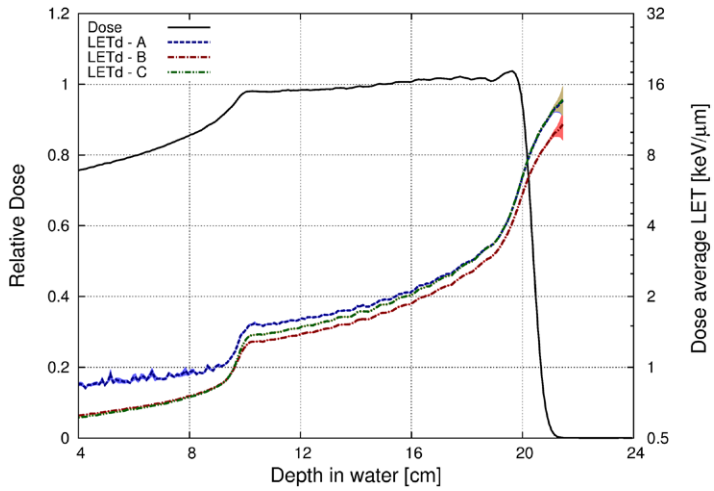

Figure 13. The same as figure 11 for an SOBP of range 20.0 cm and modulation width of 11.0 cm.

Table 2. Dose average LET values calculated by each method for various SOBPs at 80% proximal, 90% proximal, central and 90% distal depth.

SOBP			Dose average LET (keV μm^{-1})			
Range (cm)	Width (cm)	$\overline{L}_d$ method	80% proximal	90% proximal	Central	90% distal
13.0	5.9	A	1.063(11)	1.259(11)	2.574(13)	6.72(3)
		B	0.922(2)	1.166(3)	2.299(10)	5.67(2)
		C	0.919(3)	1.142(4)	2.535(13)	6.76(3)
23.5	6.2	A	1.025(10)	1.224(11)	2.328(10)	6.68(3)
		B	0.881(2)	1.097(4)	2.077(7)	5.63(3)
		C	0.878(3)	1.105(4)	2.277(9)	6.72(4)
20.0	11.0	A	0.89(3)	1.01(2)	1.94(2)	6.45(3)
		B	0.670(2)	0.833(2)	1.705(8)	5.91(3)
		C	0.666(2)	0.828(3)	1.848(11)	6.49(3)

modulation width of 13.0 cm and 5.9 cm, respectively), a high energy one for a prostate case (figure 12, with a range and modulation width of 23.5 cm and 6.2 cm, respectively) and an intermediate range SOBP (figure 13, with a range of 20.0 cm and width of 11.0 cm). The number of primary protons was such that the main pristine peak was simulated with, at least, 2×10^7 protons. The voxel thickness (Δz) was 1.0 mm and the width (Δr) was 1.0 cm. The production cut of secondary particles was 0.05 mm. Dose deposition and $\overline{L}_d$ values were calculated along the central axis. The $\overline{L}_d$ values obtained at 80% proximal, 90% proximal, central and 90% distal SOBP dose levels are presented in table 2, with statistical uncertainties, for each SOBP. Considering method 'C' as reference, since it provided the most reliable results, we observe that method 'A' yields $\overline{L}_d$ values larger than those obtained with method 'C' at depths proximal to SOBP (e.g., 80 and 90% proximal SOBP dose levels), with greater differences for wider SOBPs. For instance, $\overline{L}_d$ calculated with method 'A' was 16%, 17% and 34% larger than method 'C' for SOBP width values 5.9 cm, 6.2 cm and 11.0 cm, respectively;

however, methods 'B' and 'C' show a good agreement within uncertainties in this region. At distal SOBP, methods 'A' and 'C' agree within uncertainties, but differences of about 15% are reported between methods 'B' and 'C'.

These discrepancies are clearly connected to the results discussed previously for the 160 MeV proton beam. At depths proximal to SOBP, the residual range of protons is of several centimeters. For such a situation, we have shown that method 'A' gives $\overline{L}_{\mathrm{d}}$ values artificially larger than method 'C' (see figure 5). The same kind of discrepancy is observed here. At the SOBP, the residual range of a significant fraction of protons is short. For this fraction of the beam, the situation in terms of the proton energy spectrum is similar to that found at the Bragg peak region of the 160 MeV beam. There, method 'B' gave artificially lower $\overline{L}_{\mathrm{d}}$ values than method 'C'. Here, disagreements between $\overline{L}_{\mathrm{d}}$ calculation methods are qualitatively similar to those discussed previously in figure 5. Also, in connection with the results reported in figure 5, the deviations found upstream from the SOBP should become smaller with a larger voxel thickness, but this would increase the differences reported at the distal edge.

4. Discussion

We have found significant differences in Monte Carlo calculations of a water tank irradiated with protons at therapeutic energies between the different $\overline{L}_{\mathrm{d}}$ calculation methods presented in this work. Microdosimetry simulations were performed only with the aim of elucidating reference $\overline{L}_{\mathrm{d}}$ values from the agreement between the macroscopic ($\overline{L}_{\mathrm{d}}$) and the microscopic ($\bar{y}_{\mathrm{D}}$) calculations.

The method referred to as 'A' in this work (10) is the most intuitive and simplest calculation method of unrestricted $\overline{L}_{\mathrm{d}}$, since it involves the actual electronic energy loss and length for each individual simulation step. However, this method yields biased higher $\overline{L}_{\mathrm{d}}$ values when the condensed-history algorithm used for proton transport produces the explicit emission of δ-rays, while the proton is traveling through a voxelized geometry. As with other condensed-history Monte Carlo codes, Geant4 has a production threshold for the emission of δ-rays to avoid infrared divergence, so that secondary electrons released with an expected range below such a threshold are not tracked in the simulation, being its kinetic energy considered as deposited locally within the volume where the ionization was produced. Thus, when the transport algorithm calculates an energy transfer from the proton to an electron of the material larger than the energy threshold, the electronic energy loss of the proton after the step completion must be larger than such a threshold due to energy conservation (we recall that in Geant4 the user sets the threshold in terms of expected range and the code internally calculates the energy threshold for each pair of particle and material). However, the lengths of the steps rarely become larger than the typical voxel size, because the step definition is restricted to the boundaries of the volume in which the particle is being transported. The result of having this artificial step limitation together with collision in which the energy transferred to δ-rays is above the production threshold is the introduction of spurious high LET values associated with δ-ray-emitting steps (shown in figures 6–8) into the weighted average expressed in (10), especially in small voxels and where the energy (or residual range) of the proton beam is large enough to produce a non-negligible amount of δ-rays above the threshold. In our simulation of a water tank irradiated by a 160 MeV proton beam, a difference of about a factor of 1.8 was found for $\overline{L}_{\mathrm{d}}$ at a 4.0 cm depth if the voxel thickness was varied from 2.0 to 0.2 mm, with a production threshold of 0.05 mm (figure 5). If the production threshold becomes higher, the bias is reduced (figure 8) because the probability of δ-ray explicit tracking becomes lower and so does the impact of steps with spurious high LET associated. The presence of the bias does

not mean that the condensation technique used for proton transport is wrong, since these high-energy transfer collisions actually happen when a proton moves through a material. What the bias shows is that method 'A' proposed for $\overline{L}_d$ calculation (10) is not consistent, especially if the typical voxel size becomes smaller than 1 mm. AQ5

The calculation method 'B' (11) could be a possible solution to avoid the impact of these spurious high LET terms. Here, the LET is calculated as the fraction of the electronic energy loss over the trajectory length within the voxel. As shown in figure 5, this calculation method gives less biased $\overline{L}_d$ values than method 'A' with small voxels at depths where the residual range is larger than 5 cm, thanks to the lower impact that δ-ray-emitting steps have in the LET in terms of the weighted average (11). This small bias is a consequence of the increasing importance of energy exchange fluctuations as the voxel thickness becomes smaller (figure 9), which is related to the limitations of applying the LET concept in small volumes. Furthermore, this method has a clear tendency to decrease the $\overline{L}_d$ value near the Bragg peak position as the voxel thickness increases. This occurs because protons with a residual range smaller than the voxel size (thus high LET) have a low weighting factor (figure 10) due to the relatively short path described within the voxel; obviously this effect becomes more noticeable for larger voxel sizes. Unfortunately, we could not estimate $\overline{L}_d$ values from microscopic methods in this region, since the validity of (6) is restricted to particles with a residual range considerably longer than the site diameter (Kellerer 1985). Nevertheless, the calculation method 'B' showed a stable performance against transport parameter changes, such as the production threshold of secondary particles, in contrast to method 'A' (figure 8).

The calculation method 'C' (12) followed the step-by-step approach of method 'A' but computed the LET directly from the electronic stopping power tables. Method 'C' not only yields more stable $\overline{L}_d$ values against voxel size changes, but shows the most consistent agreement with the $\overline{L}_d$values estimated from microdosimetric calculations (figure 5). In addition, the calculations carried out with this computing strategy were not affected by changes in the production threshold of secondary particles (figure 8). Thus, method 'C' shows the most consistent performance of the three calculation methods despite the fact that it uses the LET computed from stopping power tables instead of the actual LET associated with each step, which is equivalent to ignoring the energy exchange fluctuations (actually present along the proton transport) in the LET calculations. Nevertheless, this method is consistent with the definition of LET, which is defined as the *mean* energy loss per unit path length.

We have also found qualitatively similar discrepancies for clinical SOBPs. For instance, method 'A' gave considerably larger $\overline{L}_d$values than method 'C'. Differences were greater for wider SOBPs at 80% dose level proximal SOBP, ranging between roughly 15% (5.9 cm width) and 30% (11.0 cm).

Although we expect these differences to become smaller for a voxel size greater than 2.0 mm, such differences are expected to have a significant impact on RBE estimations, especially at the entrance in patient of each treatment field. AQ6

5. Conclusions

We have compared unrestricted dose average LET values ($\overline{L}_d$) obtained by various Monte Carlo calculation methods reported in the literature to calculate dose deposition and unrestricted $\overline{L}_d$ maps in voxelized geometries exposed to therapeutical proton beams. The aim of this work has been to analyze the influence of the calculation method on the $\overline{L}_d$ value determined with Monte Carlo simulations. Since this is a pure methodological work, we decided to calculate $\overline{L}_d$ only for primary protons with the intention of simplifying the comparisons. In

a realistic calculation, contributions from secondary particles, such as secondary protons or nuclear fragments should be considered as discussed elsewhere (Grassberger and Paganetti 2011, Romano *et al* 2014).

Our main conclusion is that method 'C' (12) gave the most consistent performance among the scoring methods used in this work. This is true not only from the point of view of the calculations, but from the point of view of being a method that is less influenced by parameters that may change in the clinic from patient to patient depending on the treatment site, which is of key importance in clinical RBE estimations. Such stability is somehow a consequence of calculating the LET at each proton step as the *mean* energy loss per unit path length, in accordance with the definition of LET.

We would like to emphasize that all the calculation methods presented in this work could be implemented in other Monte Carlo codes. Although Geant4 was used in this work, the biased $\overline{L}_{\mathrm{d}}$ values obtained with methods 'A' and 'B' seem to be a consequence of the scoring method itself, which is influenced by step terminations due to boundary crossings and the presence of 'hard' collisions producing high-energy δ-rays; therefore, we expect similar results with other Monte Carlo codes using condensed-history transport algorithms. Moreover, we expect scoring method 'C' to determine stable $\overline{L}_{\mathrm{d}}$ values with other Monte Carlo codes as well.

AQ7

Acknowledgments

This work was supported in part by the Spanish Ministry of Science and Innovation under grant FPA2011-28770-C03-02 and from University of Seville under the IVPPI-US exchange program. The authors would like to thank Niels Bassler (University of Aarhus, Denmark) and Hugo Palmans (National Physical Laboratory [NPL], United Kingdom) for their useful comments. Special thanks to José Manuel Quesada (University of Seville) and Carlos Bernal (CICA, Seville, Spain) for their contribution to the management and startup of the GETERUS computing cluster hosted at CICA.

Appendix. Estimation of δ_2 and E_d from the calculation of $f_c(\varepsilon_c)$

Let us assume a microscopic site in a water medium irradiated by protons with a residual range considerably longer than the site diameter. The weighted average of energy imparted per proton single collision, δ_2, can be calculated directly from its definition (7) by Monte Carlo codes able to simulate each single interaction between protons and the medium. However, such computation is not possible with condensed-history Monte Carlo simulations, where collisions involving energy exchanges below a given threshold are computed as continuous energy loss, i.e., they are not calculated individually. In our Geant4 simulations, discrete ionization processes were calculated only if a δ-ray was released with kinetic energy above $\varepsilon_{\mathrm{min}} = 100\,\mathrm{eV}$. Consequently, it was not possible to calculate the distribution function of energy imparted per proton single collision, $f_c(\varepsilon_c)$, *below* $\varepsilon_{\mathrm{min}}$ with our approach, as shown in figure 4.

In order to overcome this limitation, we calculated δ_2 with approximation (8), in which δ_2 is estimated assuming the probability density of energy losses in single collision predicted by the free electron model, i.e., $f_{\mathrm{c}}(\varepsilon_{\mathrm{c}}) \equiv f_{\mathrm{c,free}}(\varepsilon_{\mathrm{c}}) = k / \varepsilon_{\mathrm{c}}^2$. If the range of δ-rays becomes larger than the site diameter, then the probability density of energy imparted per single collision is equal to $f_{c,free}(\varepsilon_{\mathrm{c}})$ only up to an upper limit energy value, E_{d}, which is introduced as correction to account for the efflux of energy carried out of the site by δ-rays (Kellerer 1985).

We deduced E_d as follows. Let us denote the distribution function of ε_{c} calculated with Geant4 as $f_{\mathrm{c,MC}}(\varepsilon_{\mathrm{c}})$. Since the definition of δ_2 involves the second and first moments of the

distribution, we calculated $E_{d,1}$ as the upper limit of the integral from ε_{min} of $\varepsilon_c f_{c,free}(\varepsilon_c)$ which equals the integral from ε_{min} of $\varepsilon_c f_{c,MC}(\varepsilon_c)$. We did a similar calculation with $\varepsilon_c^2 f_{c,free}(\varepsilon_c)$ and $\varepsilon_c^2 f_{c,MC}(\varepsilon_c)$ to get $E_{d,2}$:

$$\int_{\varepsilon_{min}}^{E_{d,1}} \varepsilon_c f_{c,free}(\varepsilon_c)\ d\varepsilon_c = \int_{\varepsilon_{min}}^{\varepsilon_{max}} \varepsilon_c f_{c,MC}(\varepsilon_c)\ d\varepsilon_c \equiv I_1, \tag{A.1}$$

$$\int_{\varepsilon_{min}}^{E_{d,2}} \varepsilon_c^2 f_{c,free}(\varepsilon_c)\ d\varepsilon_c = \int_{\varepsilon_{min}}^{\varepsilon_{max}} \varepsilon_c^2 f_{c,MC}(\varepsilon_c)\ d\varepsilon_c \equiv I_2\,. \tag{A.2}$$

Solving for $E_{d,1}$ and $E_{d,2}$ yields

$$E_{d,1} = \varepsilon_{min}\exp\left(\frac{I_1}{k}\right), \tag{A.3}$$

$$E_{d,2} = \varepsilon_{min} + \frac{I_2}{k}\,. \tag{A.4}$$

The value of k was deduced by fitting ${\varepsilon_c}^2 f_{c,MC}$ data between ε_{min} and $\varepsilon_c = 1.0$ keV, since we found that $\varepsilon_c^2 f_{c,MC}$ was roughly constant along this interval for all simulations. Finally, the average between $E_{d,1}$ and $E_{d,2}$ gave the value of E_d.

AQ8 ## References

Agostinelli S *et al* (Geant4 Collaboration) 2003 Geant4—a simulation toolkit *Nucl. Instrum. Methods Phys. Res.* A **506** 250–303

Allison J *et al* (Geant4 Collaboration) 2006 Geant4 developments and applications *IEEE Trans. Nucl. Sci.* **53** 270–8

Barendsen GW 1994 RBE-LET relationships for different types of lethal radiation damage in mammalian cells: comparison with DNA dsb and an interpretation of differences in radiosensitivity *Int. J. Radiat. Biol.* **66** 433–6

Bassler N, Jäkel O, Sondergaard C S and Petersen J B 2010 Dose- and LET-painting with particle therapy *Acta Oncol.* **49** 1170–6

Belli M *et al* 1998 RBE-LET relationships for cell inactivation and mutation induced by low energy protons in v79 cells: further results at the LNL facility *Int. J. Radiat. Biol.* **74** 501–9

Belli M *et al* 2000 Inactivation of human normal and tumour cells irradiated with low energy protons *Int. J. Radiat. Biol.* **76** 831–9

Berger M J, Coursey M A, Zucker M A and Chang J 2005 ESTAR, PSTAR, and ASTAR: Computer programs for calculating stopping-power and range tables for electrons, protons and helium ions
AQ9 (version 1.2.3) (http://physics.nist.gov/Star)

Burigo L, Pshenichnov I, Mishustin I and Bleicher M 2014 Microdosimetry spectra and RBE of 1H, 4He, 7Li and 12C nuclei in water studied with Geant4 *Nucl. Instrum. Methods Phys. Res.* B **320** 89–99

Carabe A, España S, Grassberger C and Paganetti H 2013 Clinical consequences of relative biological effectiveness variations in proton radiotherapy of the prostate, brain and liver *Phys. Med. Biol.* **58** 2103–17

Cortés-Giraldo M A, Quesada J M, Gallardo M I and Capote R 2012 An implementation to read and write IAEA phase-space files in GEANT4-based simulations *Int. J. Radiat. Biol.* **88** 200–8

Delaney T F and Kooy H 2008 *Proton and Charged Particle Radiotherapy* (Philadelphia, PA: Lippincott Williams and Wilkins)

Fager M *et al* 2014 *Int. J. Radiat. Oncol. Biol. Phys.* Submitted AQ10

Folger G, Ivanchenko V N and Wellisch H P 2004 The Binary Cascade—nucleon-nuclear reactions *Eur. Phys. J.* **A21** 407–17

Francis Z, Incerti S, Ivanchenko V, Champion C, Karamitros M, Bernal M A and El Bitar Z 2012 Monte Carlo simulation of energy-deposit clustering for ions of the same LET in liquid water *Phys. Med. Biol.* **57** 209–24

Frese M C, Wilkens J J, Huber P E, Jensen A D, Oelfke U and Taheri-Kadkhoda Z 2011 Application of constant vs variable relative biological effectiveness in treatment planning of intensity-modulated proton therapy *Int. J. Radiat. Oncol. Biol. Phys.* **79** 80–8

Furusawa Y, Fukutsu K, Aoki M, Itsukaichi H, Eguchi-Kasai K, Ohara H, Yatagai F, Kanai T and Ando K 2000 Inactivation of aerobic and hypoxic cells from three different cell lines by accelerated 3He-, 12C-, and 20Ne-ion beams *Radiat. Res.* **154** 485–96

GEANT4, Physics Reference Manual: www.geant4.org/geant4/support/userdocuments.shtml AQ11

Gerweck L E and Kozin S V 1999 Relative biological effectiveness of proton beams in clinical therapy *Radiother. Oncol.* **50** 135–42

Giantsoudi D, Grassberger C, Craft D, Niemierko A, Trofimov A and Paganetti H 2013 Linear energy transfer-guided optimization in intensity modulated proton therapy: Feasibility study and clinical potential *Int. J. Radiat. Oncol. Biol. Phys.* **87** 216–22

Goodhead D T *et al* 1992 Direct comparison between protons and alpha-particles of the same LET: I. Irradiation methods and inactivation of asynchronous V79, HeLa and C3H 10T½ cells *Int. J. Radiat. Biol.* **61** 611–24

Grassberger C and Paganetti H 2011 Elevated LET components in clinical proton beams *Phys. Med. Biol.* **56** 6677–91

Hawkins R B 2003 A microdosimetric-kinetic model for the effect of non-Poisson distribution of lethal lesions on the variation of RBE with LET *Radiat. Res.* **160** 61–9

IAEA 2008 Relative biological effectiveness in ion beam therapy *IAEA Technical Report Series 461* (Vienna: IAEA)

ICRU 1970 Linear energy transfer *ICRU Report 16* (Washington, DC: ICRU)

ICRU 1983 Microdosimetry *ICRU Report 36* (Bethesda, MD: ICRU)

ICRU 1984 Stopping powers for electrons and positrons *ICRU Report 37* (Bethesda, MD: ICRU)

ICRU 1993 Stopping powers and ranges for protons and alpha particles *ICRU Report 49* (Bethesda, MD: ICRU)

ICRU 1998 Fundamental quantities and units for ionizing radiation *ICRU Report 60* (Bethesda, MD: ICRU)

ICRU 2005 Stopping of ions heavier than helium *ICRU Report 73* (Bethesda, MD: ICRU)

ICRU 2011 Fundamental quantities and units for ionizing radiation (revised) *ICRU Report 85* (Bethesda, MD: ICRU)

Incerti S *et al* 2010 Comparison of Geant4 very low energy cross section models with experimental data in water *Med. Phys.* **37** 4692–708

Kantemiris I, Karaiskos P, Papagiannis P and Angelopoulos A 2011 Dose and dose averaged LET comparison of 1H, 4He, 6Li, 8Be, 10B, 12C, 14N and 16O ion beams forming a spread-out Bragg peak *Med. Phys.* **38** 6585–91

Kellerer A M 1985 Fundamentals of microdosimetry *The Dosimetry of Ionizing Radiation* vol **1** ed K R Kase *et al* (London: Academic) pp 77–161

Kempe J, Gudowska I and Brahme A 2007 Depth absorbed dose and LET distributions of therapeutic 1H, 4He, 7Li and 12C beams *Med. Phys.* **34** 183–92

Lindborg L, Hultqvist M, Carlsson Tedgren A and Nikjoo H 2013 Lineal energy and radiation quality in radiation therapy: model calculations and comparison with experiment *Phys. Med. Biol.* **58** 3089–105

Matsuura T *et al* 2010 Apparent absence of a proton beam dose rate effect and possible differences in RBE between Bragg peak and plateau *Med. Phys.* **37** 5376–81

Paganetti H and Goitein M 2001 Biophysical modeling of proton radiation effects based on amorphous track models *Int. J. Radiat. Biol.* **77** 911–28

Paganetti H, Niemierko A, Ancukiewicz M, Gerweck L, Goitein M, Loeffler J S and Suit M D 2002 Relative biological effectiveness (RBE) values for proton beam therapy *Int. J. Radiat. Oncol. Biol. Phys.* **53** 407–21

PTCOG Particle Therapy Cooperative Group www.ptcog.ch

Quesada J M, Ivanchenko V, Ivanchenko A, Cortés-Giraldo M A, Folger G, Howard A and Wright D 2011 Recent developments in pre-equilibrium and de-excitation models in Geant4 *Prog. Nucl. Sci. Technol.* **2** 936–41

Romano F, Cirrone G A P, Cuttone G, Di Rosa F, Mazzaglia S E, Petrovic I, Ristic Fira A and Varisano A 2014 A Monte Carlo study for the calculation of the average linear energy transfer (LET) distributions for a clinical proton beam line and a radiobiological carbon ion beam line *Phys. Med. Biol.* **59** 2863–82

Salvat F, Fernández-Varea J M and Sempau J 2009 PENELOPE-2008: a code system for Monte Carlo simulation of electron and photon transport *Nuclear Energy Agency Report No.* 6416 (OECD)

Schardt D, Elsässer T and Schulz-Ertner D 2010 Heavy-ion tumor therapy: physical and radiobiological benefits *Rev. Mod. Phys.* **82** 383–425

Wilkens J J and Oelfke U 2003 Analytical linear energy transfer calculations for proton therapy *Med. Phys.* **30** 806–15

Wilkens J J and Oelfke U 2004 A phenomenological model for the relative biological effectiveness in therapeutic proton beams *Phys. Med. Biol.* **49** 2811–25

QUERIES

Page 2
AQ1
Please check the usage of the term [in construction in this context].
AQ2
Please define the acronyms [PTCOG, IAEA, ROOT, NIST's ESTAR, ICRU, DNA.]
AQ3
Wouters et al 1996 cited is not provided in the references list. Please check and provide complete details.
Page 10
AQ4
Please confirm whether the word "called" can be replaced with "applied" .
Page 21
AQ5
The word [constricted has been changed to [restricted]. Please confirm that this is what you intended, otherwise amend the sentence to convey your exact meaning.]
AQ6
Please check the sense of the sentence "at the entrance in patient …."
Page 22
AQ7
We have been provided funding information for this article as below. Please confirm whether this information is correct.
Spanish Ministry of Science and Innovation: FPA2011-28770-C03-02.
Page 23
AQ8
Please check the details for any journal references that do not have a link as they may contain some incorrect information.
AQ9
Please update the publication details if appropriate in reference[Berger et al 2000].
AQ10
Please update Fager M et al if it has now been published.
Page 24
AQ11
Please update the year and publication details if appropriate in references [GEANT4, PTCOG].